Journal of Materials Chemistry A

Bipolar membrane polarization behavior with systematically varied interfacial areas in the junction region

Journal:	*Journal of Materials Chemistry A*
Manuscript ID	TA-ART-10-2020-010602.R1
Article Type:	Paper
Date Submitted by the Author:	20-Dec-2020
Complete List of Authors:	Kole, Subarna; Louisiana State University, Cain Department of Chemical Engineering Venugopalan, Gokul; Louisiana State University Bhattacharya, Deepra; Louisiana State University, Chemical Engineering Zhang, Le; Louisiana State University, Cain Department of Chemical Engineering Cheng, John; Louisiana State University and A&M College Pivovar, Bryan; NREL Arges, Christopher; Louisiana State University, Cain Department of Chemical Engineering

Bipolar membrane polarization behavior with systematically varied interfacial areas in the junction region

Subarna Kole[a], Gokul Venugopalan[a], Deepra Bhattacharya[a], Le Zhang[a], John Cheng[a], Bryan Pivovar[b], and Christopher G. Arges[a]*

[a]Cain Department of Chemical Engineering, Louisiana State University, Baton Rouge, LA 70803 USA

[b]Chemical and Materials Science Center, National Renewable Energy Laboratory, Golden, CO 80401 USA

Corresponding author e-mail: carges@lsu.edu

Keywords: bipolar membranes, soft-lithography, ion-exchange membranes, electrochemistry

Abstract

The palette of applications for bipolar membranes (BPMs) has expanded recently beyond electrodialysis as they are now being considered for fuel cell and electrolysis applications. Their deployment in emerging electrochemical technologies arises from the need to have a membrane separator that provides disparate pH environments and to prevent species crossover. Most materials research for BPMs has focused on water dissociation catalysts and less emphasis has been given to the design of the polycation-polyanion interface for improving BPM performance. Here, soft lithography fabricated a series of micropatterned BPMs with precise control over the interfacial area in the bipolar junction. Polarization experiments showed that a 2.28x increase in interfacial area led to a 250 mV reduction in the onset potential. Additionally, the same increase in interfacial area yielded marginal improvements in current density due to the junction region being under kinetics-diffusion control. A simple physics model based on the electric field of the junction region rationalized the reduction in the overpotential for water dissociation as a function of interfacial area. Finally, the soft lithography approach was also conducive for fabricating BPMs with different chemistries ranging from perfluorinated polymer backbones to alkaline stable poly(arylene) hydrocarbon polymers. These polymer chemistries are better suited for fuel cell and electrolysis applications. The BPM featuring the alkaline stable poly(terphenyl) anion exchange membrane had an onset potential of 0.84 V, which was near the thermodynamic limit, and was about 150 mV lower than a commercially available variant.

Introduction

Many low temperature electrochemical processes[1] (below 200 °C) use polymeric ion-exchange membranes (IEM) as the separator to partition two fluid compartments and/or the electrodes. Most IEM research investigates single ion conductors such as anion exchange membranes (AEMs) or cation exchange membranes (CEMs). These membranes only permit the passage of anions or cations, while being impermeable to the oppositely charged ions through Donnan exclusion[2]. A less researched variant of ion-exchange membranes, but a material that has become increasingly important, is BPMs.

BPMs consist of a CEM directly appended to an AEM[1, 3]. Because the CEM contains a polyanion and the AEM features a polycation, the oppositely charged polymers at a shared

interface have been described as an abrupt junction that is analogous to p-n junctions found in semiconductor devices[4, 5]. The opposite charges at the AEM-CEM interface imposes a local electric field that can be augmented with an externally applied electric field for dissociating water into hydronium and hydroxide ion charge carriers via second Wien effect[6-9].

Effective water splitting at the bipolar junction interface, often measured through the onset potential for water splitting and the current density for water splitting at a particular cell voltage[10], depends on bulk AEM and CEM properties as well as other factors like the type of water dissociation catalyst present at the interface and quality of polycation-polyanion interface. In the recent years, due to a wide range of IEMs with different functionalities and stabilities to choose from, it is possible to tailor BPMs specific to a particular application or operating conditions (temperature, pH)[11]. There are numerous types of water dissociation catalysts[4, 12] used in bipolar junctions and they often include materials with weakly basic or acidic moieties (e.g., poly(vinylpyridine)[13] and poly(acrylic acid)[14], graphene oxide[15-17] and metal hydroxides[10, 12, 14, 18-21]).

The quality of polycation-polyanion interface depends on the fabrication method of the BPM. Large distances between the fixed charges in the bipolar junction region, potentially caused by air bubbles or particles, deteriorate the effective width of the local electric field. The consequence of a poor interface necessitates larger cell voltages for dissociating water in BPMs. Hence, making adequate interfacial contact between the polycation and polyanion in BPMs, is paramount for minimizing BPM polarization.

From an applications standpoint, BPMs have been primarily used in electrodialysis setups for the production of mineral acids and bases[3, 22-24] from their analogue salts in water. This is particularly useful for converting concentrated waste brine from desalination processes (e.g., reverse osmosis) into acid and base chemicals used in industrial processes[25]. Other commercial uses include pH adjustment of process streams without the addition of mineral/organic acids or bases[26-29] – e.g., modifying the pH of juice or food streams without the addition of sodium, potassium, chloride, sulfate, or nitrate ions.

Electrochemical platforms for energy conversion, storage, and chemical manufacturing require continued cost reductions and improved performance and stability prior to proliferation and marketplace acceptance[30]. In niche scenarios, there are inherent advantages of using a BPM separator as opposed to an AEM or CEM separator in the said devices[12, 31-33]. First, it is important

to recognize fuel cells and electrolyzers tend to operate most effectively at pH extremes for attaining facile electrode kinetics. The use of single ion-conducting membrane separator limits the device to operate at the same pH at both electrodes. However, there are several instances of fuel cell platforms operating the electrodes at disparate pH values[12, 31-33]. For instance, low-temperature polymer electrolyte membrane fuel cells may perform hydrogen oxidation under acidic pH, which is quite facile[34]. Conversely, oxygen reduction reaction has slightly better reaction kinetics under a basic environment and has reasonable kinetics when operated with non-platinum group metal electrocatalysts[35, 36] (e.g., silver, cobalt oxides, N,P doped graphene[37], etc.). BPMs and their ability to provide pH control also offers advantages to directed borohydride fuel cells[38-41]. In the context of carbon dioxide (CO_2) electrolysis[42], a BPM is useful in preventing product crossover from the cathode to anode[43] and preventing the electrolyzer from acting as a CO_2 pump[43-45]. It is also effective as a separator in CO_2 electrolysis for forming organic acids[44].

Most materials related research about BPMs has focused on developing and evaluating water dissociation catalysts[4, 12]. BPM fabrication and manufacture[47, 48] has received less attention. The lamination of AEM and CEM together through a mechanical hot press makes it difficult to mitigate the inclusion of air bubbles at the interface that compromise BPM performance. The direct application of polycation or polyanion dissolved in solution on the oppositely charged membrane also has challenges as it requires that the one polymer be soluble (or dispersed well in a solvent) while the receiving oppositely charged membrane being insoluble to the solvent and resisting swelling during the application process. The direct application process has mainly relied upon liquid solution deposition[4, 17], aerosolized spray deposition[33, 49], or spin-coating[15] approaches. More recently, Pintauro and co-workers[10, 17], and others[50], have created intimate, 3D bipolar junctions through electrospinning a polyanion or polycation followed by depositing a water dissociation catalyst and electrospinning the oppositely charged polymer. Then, the layered electrospun mats were exposed to solvent vapor to form a compact bipolar junction. The 3D bipolar junction BPMs displayed superior performance, in terms of onset potential and current density at a particular cell voltage, when compared to a commercially available BPM (Fumasep®). Although it is recognized that increasing the interfacial surface area between the polycations and polyanions in BPMs improves the current density and onset potential for water splitting, it is unclear how these metrics scale with interfacial area.

In this work, the process of soft lithography was adopted for preparing BPMs with systematically varied interfacial areas. This methodology was inspired from previous reports that micropatterned the surfaces of CEMs (e.g., Nafion™) and AEMs for increasing the interfacial area between the electrode and membrane in catalyzed coated membranes (CCMs) used in low-temperature fuel cells[51-54]. The micropatterned CEMs from soft lithography were deposited with a water dissociation catalyst (aluminum hydroxide ($Al(OH)_3$) nanoparticles[10]) followed by a thermal-mechanical press with an AEM to prepare BPMs. To ensure adequate interfacial contact in the bipolar junction, the BPMs were solvent annealed in a custom-built flow chamber that is traditionally used for solvent annealing thin film block copolymers[55, 56]. A 4-point electrochemical cell was then used to assess the water splitting kinetics in micropatterned and non-patterned BPMs[10, 15]. Notably, a 2.28x increase in the interfacial area within the bipolar junction of the BPM caused a 250 mV reduction in the onset potential. These observations were rationalized by the larger interfacial areas in the bipolar junction region enhancing the junction region's electric field. With respect to current density, only very high surface area interfaces (e.g., 2.28x increase) resulted in improved current density (20 to 50%). The limited increase in current density was attributed to water diffusion limitations to the junction region. Finally, this report shows that the scalable and simple soft lithography manufacturing method was successful in making BPMs with different chemistries ranging from perfluorinated polymer backbone AEMs[57] and CEMs[58] to alkaline stable, ether free poly(arylene) hydrocarbon AEMs[59, 60]. These polymer chemistries are better suited for fuel cell and electrolysis environments that operate at elevated temperatures (60 to 95 °C) and harsher chemical environments (e.g., extreme pH and oxidizing conditions).

Results

Table 1. Properties of AEMs and CEMs used in BPMs

Membrane	SPEEK	QAPSf	Nafion™	PF AEM	ORION AEM
Thickness (μm)	26.7±3.8	37.3±6.4	24.7±3.0	28.3±3.5	37.0±3.6
σ (mS cm^{-1}) [a]	110±1.0	59±1.2	100±0.1	15±0.5	50±0.0
ASR (Ω-cm^2)[a]	0.025±0.0	0.063±0.01	0.025±0.0	0.189±0.03	0.074±0.0
Transference number[b]	0.96±0.0	1.00±0.0	1.00±0.0	0.96±0.1	0.80±0.0
Permselectivity[b]	0.94±0.0	1.00±0.0	1.00±0.0	0.94±0.1	0.70±0.1
IEC (meq g^{-1}) [b]	1.65±0.06	2.34±0.02	0.91[c]	0.91[c]	2.1[c]
Water uptake (%)[b]	5.0±5.3	38.4±2.5	51.4±37.3	27.6±2.7	11.8±2.2

[a]Measured in the proton or hydroxide ion form; [b]Measured in the sodium ion form or chloride ion form; [c]Value provided by the manufacturer

Table 1 presents the individual properties of AEMs and CEMs used to fabricate BPMs. These properties include membrane thickness, ionic conductivity, transference number and permselectivity for the counterion, ion-exchange capacity (IEC), and water uptake. **Figure S1** gives the chemical structure of AEMs and CEMs used to fabricate BPMs. The individual AEMs and CEMs are below 50 μm in thickness and the resulting BPMs are less than 125 μm in thickness. The commercial baseline variant, the Fumasep® BPM from Fumatech, was 195 μm thick. **Table S1** provides the thickness values for all BPMs studied in this report. Surface patterning did not significantly alter the BPM thickness (< 8% than the average value for all BPMs prepared for a given chemistry). Thicker membranes have the undesired consequence of greater area specific resistance (ASR) values that can compromise cell efficiency. Further, the poly(arylene ether) and perfluorinated AEMs and CEMs have permselectivity values over 0.9 making them excellent candidates for mitigating co-ion leakage in electrochemical cells. The Orion AEM had a slightly lower permselectivity value (0.8). Despite this shortcoming, it will be shown later that this AEM paired with the more permselective SPEEK results in a BPM with low co-ion leakage and thus minimal crossover current. The ionic conductivity in every variant is over 15 mS cm^{-1} in DI water. Using the ionic conductivity values and the membrane thickness values, the ASR values were

calculated (**Table 1**) and the highest ASR value was 0.189 Ω-cm^2. It is worth noting that the ohmic drop from the BPMs composed of individual AEMs and CEMs will be regulated by the highest ASR value of the CEM or AEM material in the BPM. This is caused by iso-neutrality constraints. For instance, every proton gated from the CEM side in a BPM is accompanied by a hydroxide ion from the opposite AEM side. The limitation of ion migration will be important for understanding BPM performance in the mixed control region of the polarization curves. Overall, the ASR values, as well as the low water uptake values, demonstrate that the AEMs and CEMs are good candidates for fabricating BPMs.

(a)

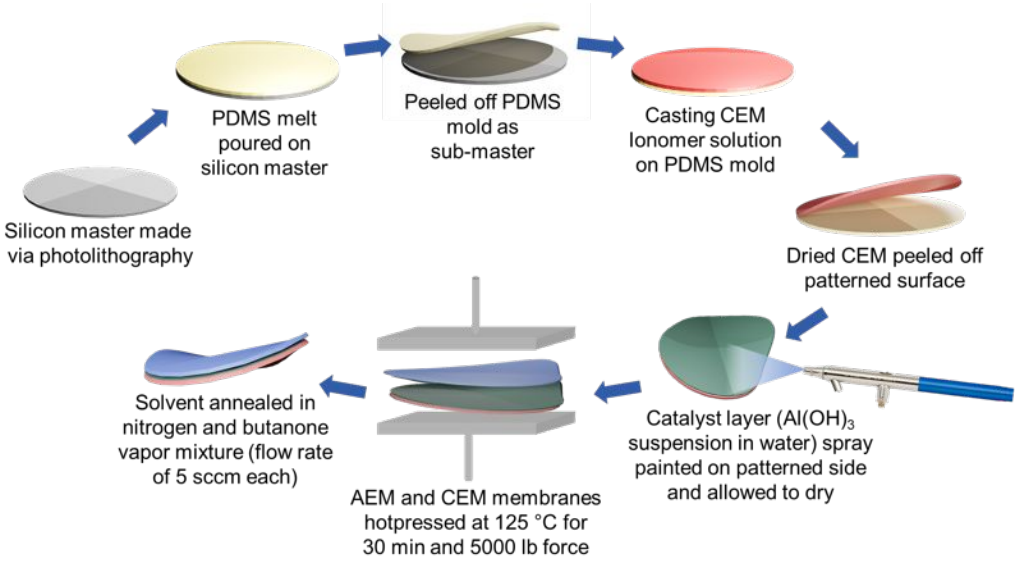

(b)

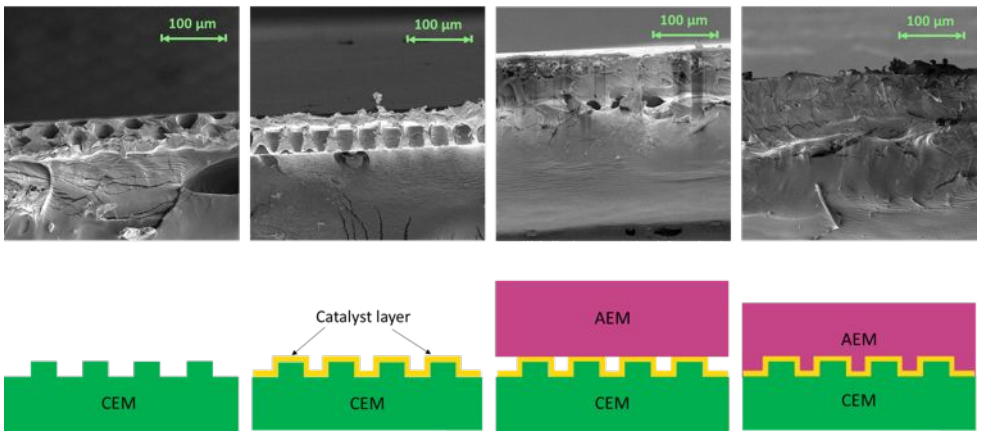

(c)

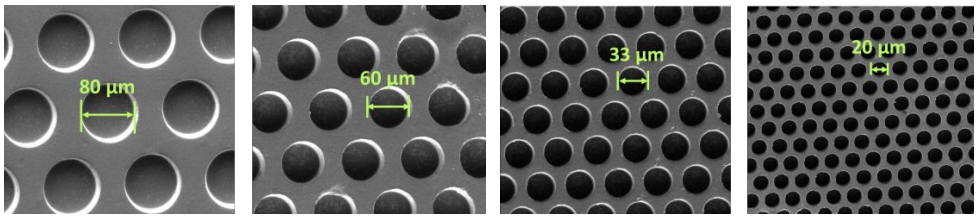

NIA = 1.19 **NIA = 1.48** **NIA = 1.95** **NIA = 2.28**

Figure 1. (a) Process flow for fabricating micropatterned BPMs with systematically varied interfacial areas in the junction region. (b) Electron micrographs of the membranes' cross-section at each stage of the SPEEK/QAPSf hydrocarbon BPM fabrication process: SPEEK CEM with topographical patterns, after spray deposition of catalyst layer on patterned side, thermal-mechanical press of SPEEK CEM and QAPSf AEM (formation of BPM), and after solvent annealing the BPM. (c) Electron micrographs of the surface of micropatterned SPEEK with different well diameters. Below these micrographs, the normalized interfacial area (NIA) values are provided. Smaller feature sizes gave larger normalized interfacial area values.

(a)

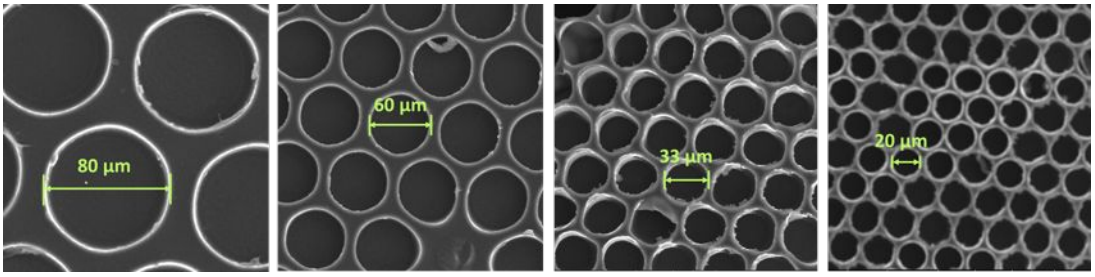

(b)

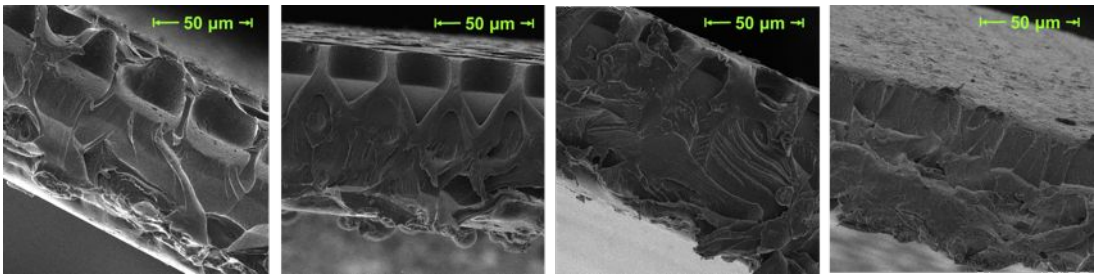

(c)

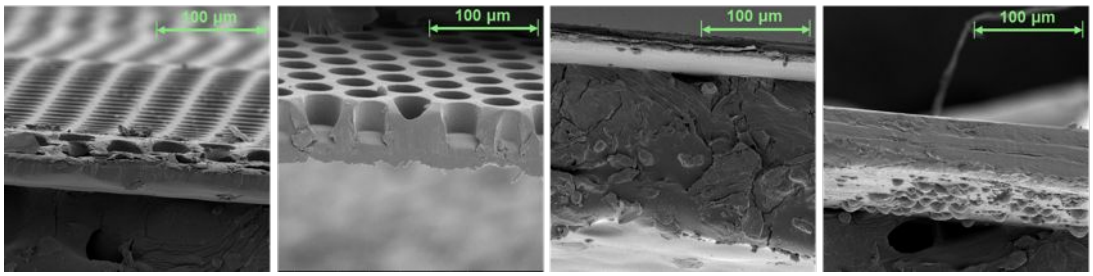

Figure 2. (a) Electron micrographs of the surface of micropatterned Nafion™ with different well diameters. (b) Cross-sectional electron micrographs at each stage of the all perfluorinated BPM fabrication process: Nafion™ CEM with topographical patterns, after spray deposition of catalyst layer on patterned side, thermal-mechanical press of Nafion™ with PF AEM, and after solvent annealing the BPM. (c) Cross-sectional electron micrographs at each stage of the SPEEK/Orion hydrocarbon BPM fabrication process: SPEEK CEM with topographical patterns, after spray deposition of catalyst layer on patterned side, thermal-mechanical press of SPEEK with Orion AEM (formation of SPEEK/Orion BPM), and after solvent annealing the BPM.

The availability of selective and low-resistant AEMs and CEMs made it possible to fabricate BPMs with systematically varied interfacial areas using soft-lithography. In this report,

a particular interfacial area value is expressed as the normalized interfacial area (NIA) value – which is the interfacial area divided by the geometric area calculated from the geometry of the silicon template. Previous research has shown that direct thermal lamination of AEMs and CEMs can lead to poor performing BPMs when compared to direct drop casting or spray deposition of one type of ion-containing polymer onto the oppositely charged polymer membrane. Initial studies attempted the spray deposition approach to fabricate BPMs using a quaternary benzyl ammonium poly(2,6-dimethyl 1,4-phenylene oxide) (QAPPO)[61] dissolved in a water-2-propanol mixture (1 to 5 wt% in a 50:50 solvent mixture). However, the water-alcohol mixture containing QAPPO swelled the receiving SPEEK CEM during BPM fabrication. Similarly, the dilute PF AEM solutions (1 to 5 wt% in an alcohol-water-DMAc 40:40:20 mixture) swelled the receiving Nafion^{TM} CEM. Due to these challenges, the direct spray deposition approach was abandoned, and the drop casting approach was not pursued further.

To produce mechanically robust and high quality BPMs, a thermal-mechanical lamination process was adopted followed by solvent vapor annealing to ensure good interfacial contact between the polycation and polyanion in the junction region. **Figure 1a** depicts the flow process for fabricating BPMs with planar and topographical patterned interfaces. For controlled studies that generated BPMs without a water dissociation catalyst, the spray deposition step of $Al(OH)_3$ in water on top of the CEM was skipped. Additionally, the solvent vapor annealing step was skipped for controlled studies that examined BPMs without the additional processing step to ensure good interfacial contact between the oppositely charged polymers.

Figure 1b provides the cross-sectional SEM images of: i.) SPEEK CEM with topographical patterns, followed by spray deposition of $Al(OH)_3$ nanoparticles on to the SPEEK CEM, thermal-mechanical pressing the SPEEK CEM with a QAPSf AEM, and then solvent vapor annealing of the resultant BPM. The cross-sectional SEM image of the micropatterned SPEEK-QAPSf BPM after the thermal-mechanical press demonstrates that the QAPSf did not fill in the topographical wells in the CEM completely. The presence of the topographical features in these electron micrographs demonstrate that surface patterns, and their interfacial area, are maintained after thermal-mechanical pressing. Hence, the NIA values calculated from the geometric patterns observed on the CEM surfaces were used for probing how interface area affects water splitting in BPMs in subsequent experiments. However, the thermal-mechanical pressing process may have

slightly altered the NIA values. After solvent vapor annealing, the surface patterns are no longer observed in the cross-sectional SEM image and a compact interfacial polycation-polyanion layer (i.e., a bipolar junction) was formed.

The generation of topographical patterns on SPEEK and Nafion™ were produced from PDMS molds that were generated from soft lithography techniques[62-64]. The surface patterns of the CEMs were defined by chromium mask used in the photolithography exposure step. **Figure 1c** shows top-down SEM images of SPEEK with 80, 40, 33 and 20 μm topographical well diameters and the resultant NIA values they produce. A smaller well diameter generates a larger NIA value.

Figure 2a shows SEM surface images of micropatterned Nafion™. **Figure 2b** provides the cross-sectional SEM images during the fabrication of all-perfluorinated BPMs from Nafion™ and PF AEM. **Figure 2c** shows the cross-sectional SEM images during the fabrication of a hydrocarbon, alkaline resilient BPM with Orion AEM paired with SPEEK. **Figure S2a** presents pictures of SPEEK/QAPSf individual membranes and resulting BPM. **Figure S2b** presents pictures of other BPMs used in this work.

An advantage of the PDMS molds generated by the soft lithography process is that they are reusable and can be used with both CEM chemistries of SPEEK and Nafion™. They can also be used with the AEM chemistries of QAPSf, PF AEM, Orion AEM, and QAPPO. Each one of these AEM or CEM chemistries were dissolved in either NMP, DMAc, DMF, alcohol, or alcohol-water mixtures. The PDMS molds maintain their structures and integrity with those solvents.

Overall, **Figures 1** and **2** demonstrate a versatile and robust process to produce CEMs with systematically defined topographical micropatterns that are subsequently used to fabricate BPMs with good interfacial contact. Systematically changing the surface pattern feature size allowed control over the NIA value in the bipolar junction region in BPMs. Additionally, the resultant PDMS mold from soft lithography were compatible with a multitude of AEM and CEM chemistries and solvents used to dissolve those polymers.

(a)

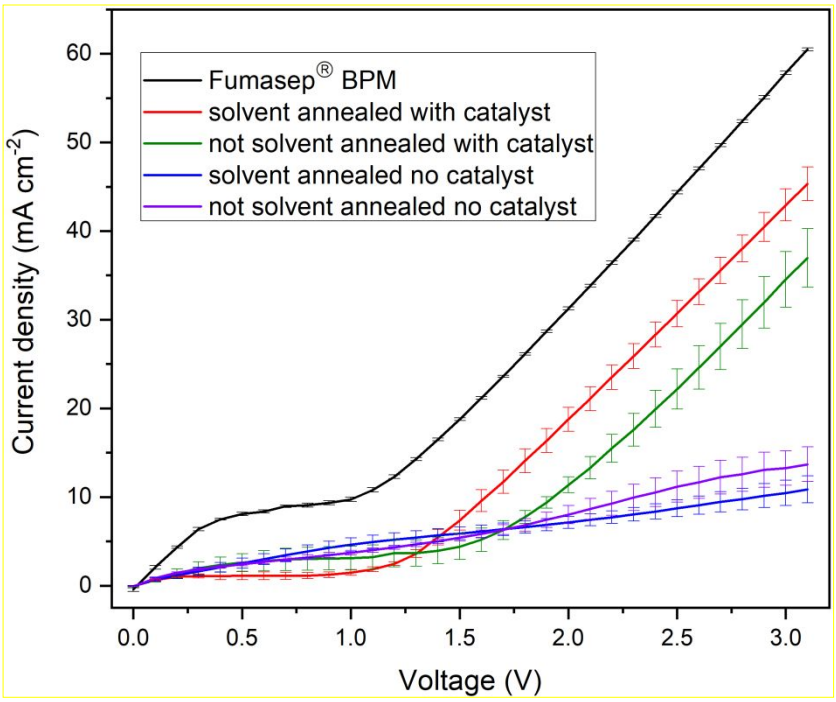

(b)

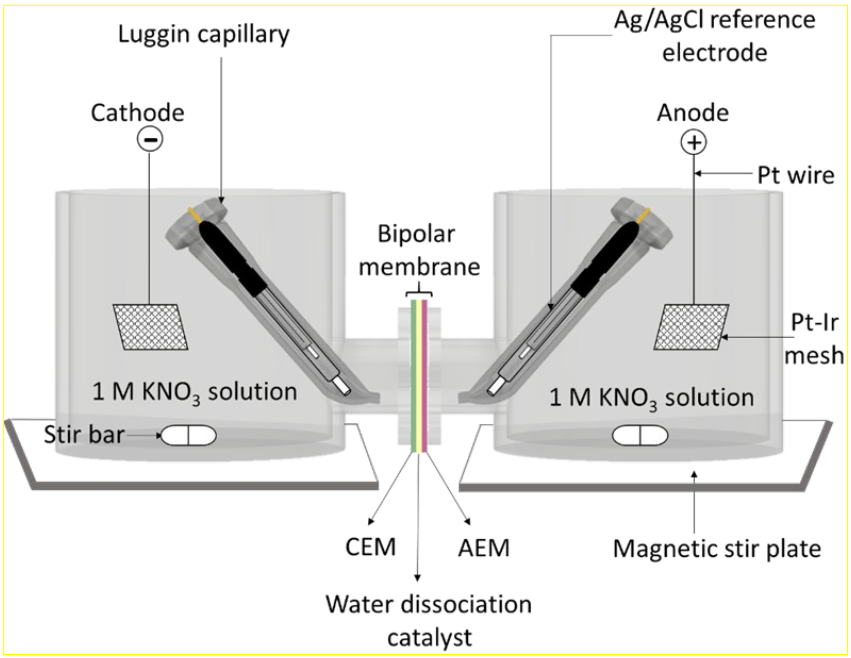

Figure 3. (a) Polarization curves for non-patterned (i.e., planar interfaces) SPEEK/QAPSf BPMs with and without $Al(OH)_3$ nanoparticle water dissociation catalysts and with and without solvent vapor annealing processing. Error bars correspond to the standard error for n=3 independent samples; (b) Schematic of the 4-point cell used to evaluate BPM polarization behavior.

Prior to exploring how interfacial area of bipolar junction interfaces impact the Figures of Merit for BPM performance, it is necessary to discuss the importance of a water dissociation catalyst and solvent vapor annealing on BPM performance. **Figure 3a** presents the polarization behavior of a commercially available BPM, Fumasep®, and 4 different types of SPEEK/QAPSf variants with planar interfaces that featured no water dissociation catalyst and a water dissociation catalyst, and that were solvent vapor annealed and non-annealed. **Figure 3b** illustrates the 4-pt cell setup used to collect polarization experiments. A picture of this cell is given in **Figure S3a**. **Figure S3b** shows the anticipated polarization behavior of bipolar membranes based upon theory and literature precedent[65] for bipolar membrane electrodialysis. The current response before the onset potential (below 1-1.5V), which typically becomes flat and mimics a limiting current, hails from the diffusion of co-ion crossover. The higher the permselectivity of the polymers used in the BPM resulted in BPMs with a low crossover current density value. To illustrate how electrolyte crossover impacts polarization behavior, a BPM with sub-mm hole was tested in the 4-point cell setup. The presence of a small hole gave a linear current response across the BPM voltage drop (**Figure S4**), and this crossover current obfuscates the contribution from water-splitting in the BPM (i.e., no limiting current can be seen before the onset potential for water splitting).

With respect to the SPEEK/QAPSf BPMs that did not contain a water dissociation catalyst, both BPMs displayed low current responses (< 15 mA cm^{-2}) in **Figure 3a** across the voltage range up to 3 V. Additionally, onset potentials for these BPMs were not clearly apparent as a rapid increase in current was not observed over the voltage range. Comparing the BPMs with a catalyst at the bipolar junction interface (SPEEK/QAPSf and Fumasep® BPM) to those without a catalyst (SPEEK/QAPSf), demonstrates that a water dissociation catalyst greatly increases water splitting in the bipolar junction region. Note: **Figure S5** shows that $Al(OH)_3$ nanoparticle catalyst loading at the BPM interface (patterned and not-patterned) does not impact the polarization behavior for SPEEK/QAPSf BPMs.

The other key observation in **Figure 3a** is that solvent vapor annealing of the planar interface SPEEK/QAPSf BPMs reduced the onset potential by 300 mV and increased the current density response by 70 % at 2 V (to 19 mA cm^{-2} from 11 mA cm^{-2}). As seen in **Figure 1b** for the micropatterned SPEEK/QAPSf BPM variants, solvent vapor annealing allows for improved interfacial contact between the polycation and polyanion in the junction region. The solvent vapor annealing process plasticizes[66] the individual AEMs and CEMs at the interface allowing these

polymers to interpenetrate and improves interfacial contact. This improved interfacial contact renders a greater concentration of effective bipolar junctions that work in tandem with the water dissociation catalyst to reduce the energy barrier for water splitting. The mathematical scaling relationships between effective bipolar junction concentrations and the onset potential for water splitting will be elaborated on in greater detail for the BPMs with systematically varied interfacial area values.

It is important to note that the current density and onset potential for water splitting of the SPEEK/QAPSf BPM is comparable or exceeds values mentioned in the literature[7-16]. There are a few instances where current density values can be substantially higher (e.g. a few hundred mA cm^{-2})[10,15], but this is most likely attributed to the cell design - which is often custom built as no commercially available BPM testing cells exist. Hence, the newly fabricated BPMs were benchmarked against a commercially available material (e.g., Fumasep® BPM by Fumatech). **Table S2** provides BPM performance values from the literature – including data on Fumasep® BPM by other groups. The data on the benchmark material varies because the testing setup is not the same between groups (e.g., the supporting electrolyte and working electrodes between studies are not the same).

Overall, **Figure 3a** highlights the importance of water dissociation catalysts and interfacial contact for producing functional BPMs. Without a water dissociation catalyst, SPEEK/QAPSf BPMs perform extremely poorly. The good interfacial contact in the bipolar junction region of SPEEK/QAPSf BPMs, enabled by solvent vapor annealing, leads to a substantial reduction in onset potential and increase in current density. However, the best performing SPEEK/QAPSf BPM with a planar interface had a higher onset potential, by 200 mV, and lower current response than the Fumasep® BPM. Despite these shortcomings, the SPEEK/QAPSf had greatly reduced co-ion leakage values compared to Fumasep® BPM. This indicates that the SPEEK/QAPSf would be better at curtailing crossover current in electrochemical devices. The lower co-ion leakage of the SPEEK/QAPSf hails from their good permselectivity values (> 0.9; **Table 1**). The next section will show that BPMs can be improved further by increasing the bipolar junction interfacial area through micropatterning the membrane surfaces and adopting alternative AEM chemistries.

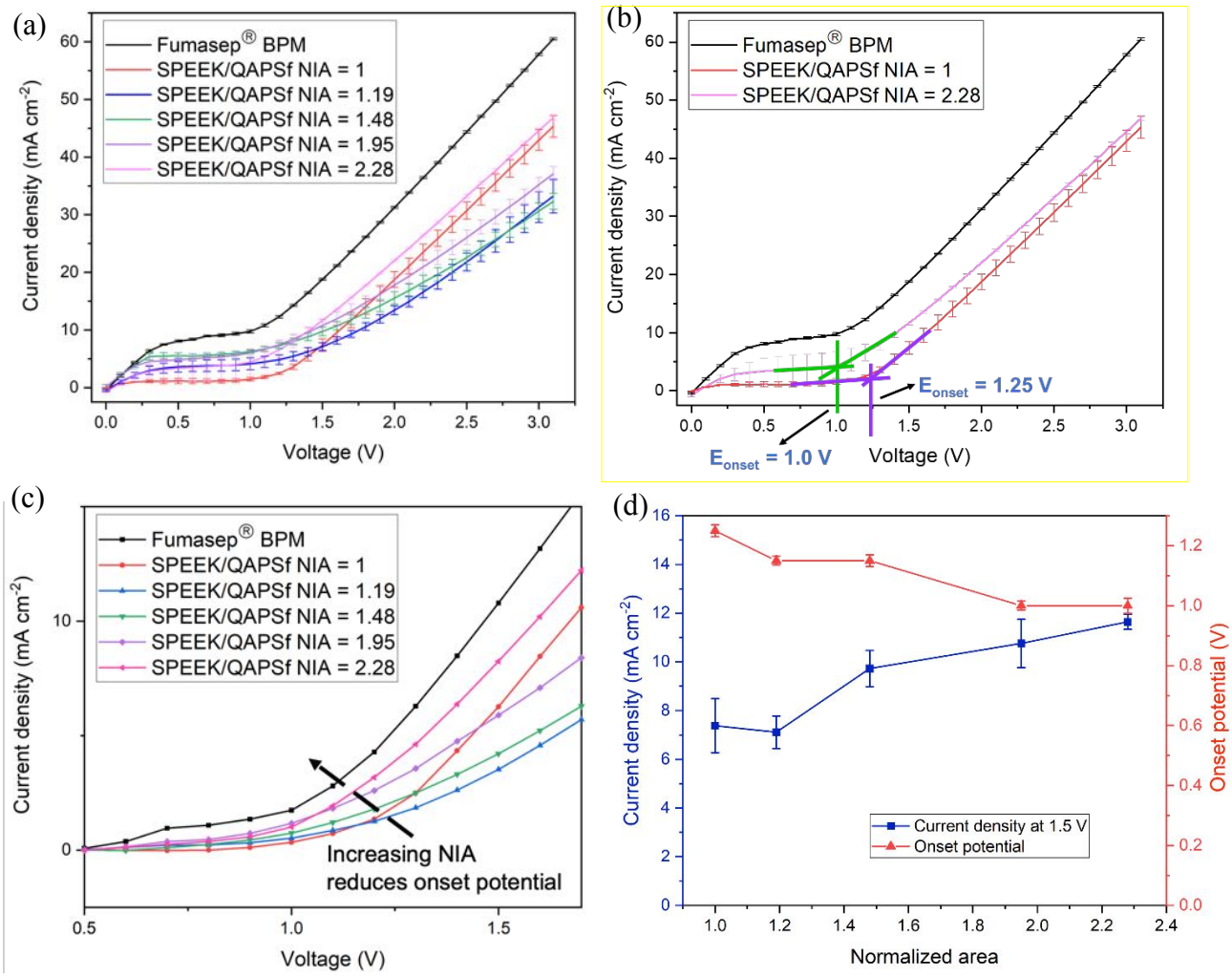

Figure 4. a.) Polarization curves for micropatterned and non-patterned SPEEK/QAPSf BPMs and Fumasep® BPM. The legend provides the NIA values with respect to the non-patterned, planar SPEEK/QAPSf BPM interface. b.) Onset potential determination for patterned SPEEK/QAPSf BPMs with NIA = 1 and 2.28. c.) Polarization curves for micropatterned and non-patterned SPEEK/QAPSf BPMs and Fumasep® BPM with crossover current subtracted. This plot is zoomed in near the onset potential and error bars are removed for clarity. Increased NIA values for the SPEEK/QAPSf BPMs reduced the onset potential) d.) The onset potential (right y-axis) and current density values at 1.5 V (left y-axis) for SPEEK/QAPSf BPMs versus NIA values. Note: All SPEEK/QAPSf BPMs contained an $Al(OH)_3$ water dissociation catalyst and were solvent vapor annealed. Error bars correspond to the standard error for n=3 independent samples.

(a)

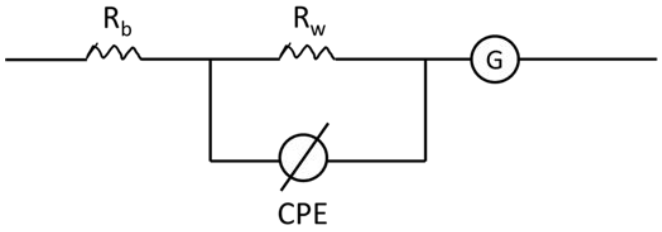

(b)

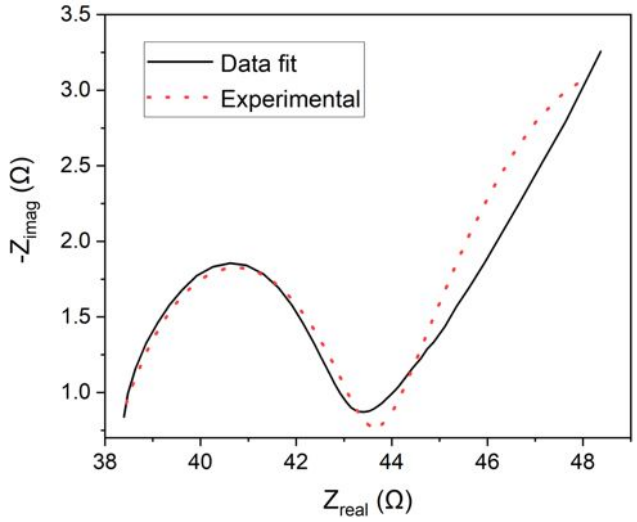

(c)

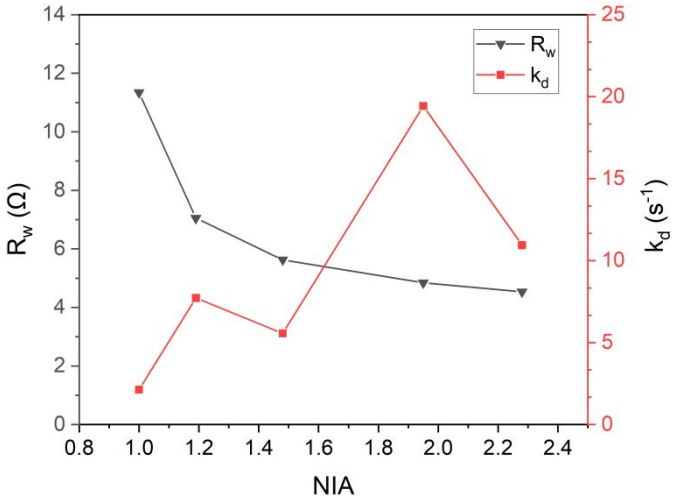

Figure 5. a.) Electrochemical equivalent circuit (ECE) used to model water dissociation in a BPM. b.) Nyquist plot of representative EIS data of water splitting in SPEEK/QAPSf patterned BPM with ECE model fit. (NIA=1.95) c.) Plot of R_w and k_d^{app}(apparent, forward water dissociation reaction rate constant) versus NIA value.

Figure 4a presents the polarization curves for water splitting of SPEEK/QAPSf BPMs with different NIA values. This Figure also contains the polarization behavior of the Fumasep® BPM as a reference. **Figure 4b** gives the polarization curves for the SPEEK/QAPSf BPM at NIA values of 1 and 2.28 (i.e., smallest and largest only) to highlight how the extreme of NIA values affect onset potential. Because each BPM displayed some current contribution from ionic species crossover (i.e., the limiting current observed before the onset potential), **Figure 4c** subtracted the crossover current contribution from the polarization data. It is clear from **Figures 4b** and **4c** that the BPM with larger interfacial areas had a smaller onset potential.

Figure 4d plots onset potential and current density for water splitting at 1.5 V from polarization experiments with SPEEK/QAPSf BPMs that have systematically varied NIA values (**Figures S6a-e** provides the determined onset potential for individual BPM curves). **Figure S7** shows the method for determining the onset potential from polarization curves. **Figure 4d** conveys a 250 mV reduction in the onset potential when increasing the NIA values to 1.95 and 2.28. This Figure also demonstrates 20% to 50% larger current density values at 1.5 V for most BPMs when increasing NIA values (i.e., NIA = 1.48, 1.95, and 2.28); however, the current density at larger cell voltages (e.g., 2 V and 3 V) only occurred for NIA = 2.28. This observation will be discussed in greater detail in the Discussion Section as the current density is both a function of reaction kinetics and diffusion.

To better understand the changes in resistances and water splitting kinetics in the bipolar junction region, *in-situ* EIS was carried out with a background voltage of 2 V. EIS with this background voltage ensured the BPM was splitting water and was in the mixed-controlled regime. The electric circuit equivalent (ECE) model (**Figure 5a**) proposed by Mallouk and co-workers[17] was adopted for extracting the resistance value associated with water splitting (R_w) and the circuit element, Gerischer element (R_G), that included both the apparent water dissociation reaction constant (k_d^{app}) and diffusion coefficient of ions (D_{ion}) away from the bipolar junction interface. R_G scales to approximately ~ $1/\sqrt{k_d^{app} D_{ion}}$. It is assumed that micropatterning the surface of the membranes does not impact bulk transport properties of the membranes, such as D_{ion}, and thus any reduction in R_G is primarily ascribed to a larger k_d^{app} value. **Figure 5b** shows the ECE model fit to the Nyquist plot from a micropatterned SPEEK/QAPSf BPM (NIA of 1.95) with a water dissociation catalyst and that was solvent annealed. **Figure 5c** plots R_w and the k_d^{app} as a function of the normalized area in the bipolar junction of the BPMs. k_d^{app} was extracted from the Gerisher

element and data fitting of the impedance data in the low frequency regime (**Figure S8**). R_w decreased with increasing interfacial area and it was inversely commensurate (i.e., a 2x increase in NIA gave a 50% reduction in R_w). k_d^{app} was also promoted with increasing interfacial area, especially when examining NIA values greater than 1; but sometimes it decreased from one NIA value to the other (e.g., it went down from NIA = 1.95 to NIA = 2.28). Similar to observations made by Mallouk and co-workers[17], the reduction in R_w correlated better with improved water-splitting in BPMs rather than k_d^{app}. Their work also showed similar water splitting performance between a 3D electrospun BPM versus a 2D BPM despite the 3D electrospun BPM having 2x to 3x lower k_d^{app} value. Hence, k_d^{app} extracted from electric circuit equivalents featuring a Gerischer element may not be a good parameter for understanding BPM water splitting kinetics and motivates future work that probes k_d^{app} in bipolar junction regions.

(a)

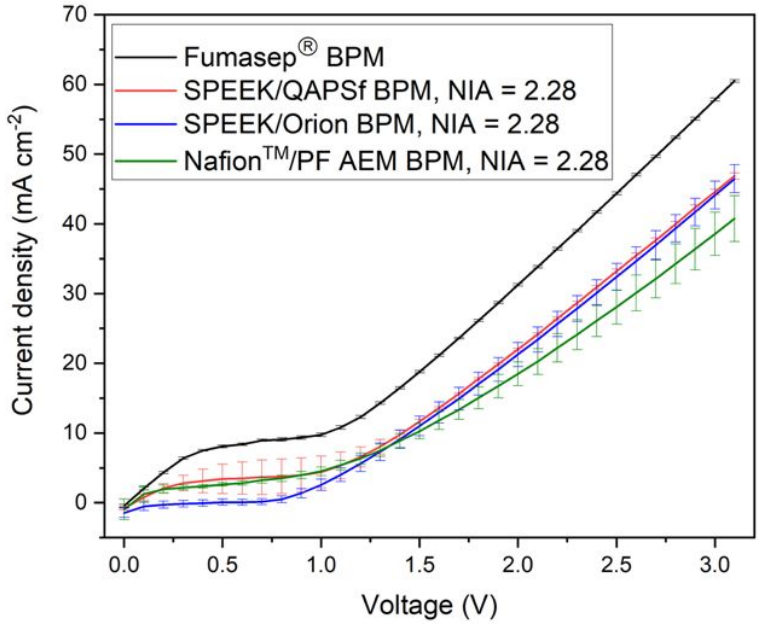

(b)

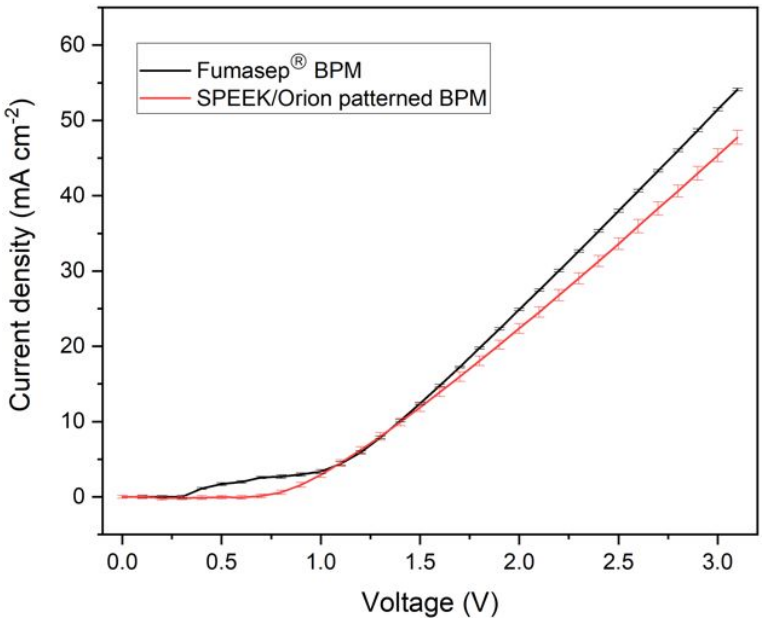

Figure 6. (a) Polarization curves for micropatterned BPMs with different membrane chemistries. (b) Polarization behavior of Fumasep® and SPEEK/Orion AEM BPMs with the crossover current subtracted.

Figure 6a conveys polarization behavior of following micropatterned BPMs (NIA = 2.28): Nafion™/PF AEM, SPEEK/QAPSf, and SPEEK/Orion AEM. These BPMs all had $Al(OH)_3$ as a water dissociation catalyst and were solvent annealed. The impetus of fabricating BPMs with PF

AEM and Orion AEM hails from their excellent alkaline stability in 1 M KOH or greater at temperatures of 80 °C for prolonged periods of time[57, 59, 60, 69]. QAPSf is known to suffer from backbone[70] and cation degradation[71] in 1 M KOH at 60 °C and a similar variant has only been shown to be stable in 2 M NaOH at 40 °C[72]. Work by Pintauro and co-workers has used quaternary ammonium benzyl poly(2,6-dimethyl 1,4-phenylene oxide) (QAPPO) AEMs in their BPMs. This AEM chemistry is also unstable in 1 M KOH at 60 °C[61, 73]. Hence, functional BPMs have been fabricated with alkaline resilient AEMs.

From **Figure 6a**, the SPEEK/Orion AEM BPM had the lowest onset potential (0.84 V) of all the BPMs tested – including 150 mV lower than the commercial Fumasep® BPM. The observed onset potential for the SPEEK/Orion AEM BPM is near the thermodynamically predicted value based upon the water dissociation constant (K_w). The excellent polarization behavior of SPEEK/Orion AEM BPM may be partially ascribed to the Orion AEM's low water uptake leading to less swelling of the BPM interface; and thus, maintenance of quality interface that has good contact[74]. The micropatterned all-perfluorinated BPM from Nafion™/PF AEM displayed similar polarization as the micropatterned SPEEK/QAPSf BPM up to 1.3 V. After 1.3 V, the all-perfluorinated BPM gave a smaller increase in current when ramping up the voltage. The lower IEC values of the perfluorinated materials give rise to a lower E_{loc} value. Plus, the higher ASR values of the PF AEM incurred a larger ohmic penalty when extracting greater current density values. It is important to note that the linear regime after the onset potential in polarization curves corresponds to mixed control (i.e., it is governed by both reaction kinetics and diffusion of water to the interface and migration of ions away from the interface).

Although the current density values are larger for Fumasep® BPM in **Figure 6a**, it is also apparent that the crossover current is quite large for Fumasep® BPM and negligible for SPEEK/Orion AEM BPMs. **Figure 6b** plots the polarization behavior of Fumasep® BPM and SPEEK/Orion AEM BPMs with the crossover current contribution subtracted. This plot demonstrates that the SPEEK/Orion AEM BPM gives current density values for water-splitting that are similar to the Fumasep® BPM up to 1.5 V. Hence, the newly prepared BPMs dissociate water to hydroxide ions and hydronium ions as well as the commercial baseline material. Additionally, it is important to recognize that the micropatterned SPEEK/Orion AEM BPM has a

lower crossover current values when compared to Fumasep® and this is an important quality for current utilization in BPM electrodialysis.

Finally, it is important to highlight that the Nafion™/PF AEM, SPEEK/Orion and SPEEK/QAPSf BPMs are composed of perfluorinated or poly(arylene) chemistries that are known to tolerate chlorine solutions[75]. The oxidative stability of these BPMs allows the use of cleaning solutions to overcome fouling problems such as bio-films and/or surfactants. Overall, the SPEEK/Orion AEM BPM and all-perfluorinated BPMs are promising candidates for applications that require harsh environments (e.g., extreme pH values, oxidizers, and elevated temperatures).

Discussion

This section shows how interfacial area amplifies the local electric field resulting in a lower onset potential (E_{onset}) for water splitting, and it also demonstrates the relation between current density with k_d^{app} and diffusion coefficient values. Prior to using mathematics to describe the local electric field as a function of interfacial area, it is important to define E_{onset} (**equation 1**) – which is equal to the sum of water dissociation overpotential (η_{WD}) and the junction potential (E_j). The latter term is described by thermodynamics (**equation 2**). η_{WD} is the difference between E_{onset} and E_j and is a proxy for the activation energy barrier for water dissociation. E_j is primarily defined from the water dissociation constant (K_w), but it is also known to have contributions from the activity of protons and hydroxide ions in the bipolar junction region. If these activity values are near one, then E_j is dependent upon temperature and K_w. When experiments are performed near 25 °C, E_j simplifies to -0.83 V. This value represents the oft-used thermodynamic minimum for water splitting in bipolar junctions[76].

$$E_{onset} = E_j + \eta_{WD} \quad (1)$$

$$E_j = \frac{RT}{F} ln(a_{H+}^{PEM} a_{OH-}^{AEM}) - \frac{RT}{F} ln(K_w) \quad (2)$$

As seen in the polarization curves in **Figures 3**, **4a**, and **6a**, the E_{onset} for water splitting is above the thermodynamic minimum of 0.83 V. As previously stated, the difference between the E_{onset} and E_j can be accounted for by η_{WD}. We posit that η_{WD} is a function of the local electric field (E_{loc}) strength in the bipolar junction region. In this derivation, E_{loc} is shown to capture the concentration of fixed charge groups, the interfacial area, and depletion width. Increasing E_{loc}

alleviates the applied voltage in the cell needed for water splitting in BPMs. E_{loc} as a function of interfacial area was derived from the Poisson equation (**equations 3** to **7**). This equation has been traditionally used to relate the concentration of oppositely aligned charges in the electrochemical double layer[77], which is analogous to bipolar junction interfaces in BPMs, to electric field strength. The Poisson-Boltzmann equation was not used because the ionic charges in the bipolar junction region are fixed in position since they are tethered to the backbone and the counterions cannot migrate far from the fixed charges. Hence, the concentration of ionic charges is independent of the local potential and can be treated as a constant with respect to position and electric potential.

$$\nabla^2\phi_{BPJ} = -\frac{\rho_{BPJ}}{\varepsilon} \quad (3)$$

The Poisson equation (**equation 3**) can be integrated over the control volume of oppositely fixed charges in intimate contact leading to the gradient of the electric potential (i.e., E_{loc}). It is assumed that the permittivity ($\varepsilon = \varepsilon_r \varepsilon_0$, dielectric constant multiplied by the vacuum permittivity constant) and the density of fixed charges (ρ_{BPJ}) are constant for a particular membrane chemistry (influenced by the water uptake and IEC).

$$\int_V \nabla^2\phi_{BPJ}\mathrm{dV} = -\int_V \frac{\rho_{BPJ}}{\varepsilon} dV \quad (4)$$

$$\nabla\phi_{BPJ} = E_{loc} = -\frac{\rho_{BPJ}}{\varepsilon}\int_V dV \quad (5)$$

The integral of the control volume can be approximated by the product of the interfacial area (A_{int}) and depletion width thickness (t_{dw}).

$$\int_V dV = V = A_{int} \cdot t_{dw} \quad (6)$$

The t_{dw} is defined as the separation distance from one fixed charge to the oppositely fixed charge that still renders an effective electric field. The t_{dw} can be estimated using a simple electrostatic derivation[76] and the known density of fixed charges. It was also shown in the work of Mallouk and co-workers that the incorporation of a water dissociation catalyst shrinks the depletion width but enhances the k_d^{app} and lowers the R_w[17]. Shrinking R_w through the incorporation of a water dissociation catalyst had a more pronounced effect on improving water splitting in BPMs than having larger depletion widths. With the control volume estimated and rewritten as a function of A_{int} and t_{dw}, the following expression emerges for $E_{loc.}$

$$E_{loc} = -\frac{\rho_{BPJ}}{\varepsilon} \cdot A_{int} \cdot t_{dw} \quad (7)$$

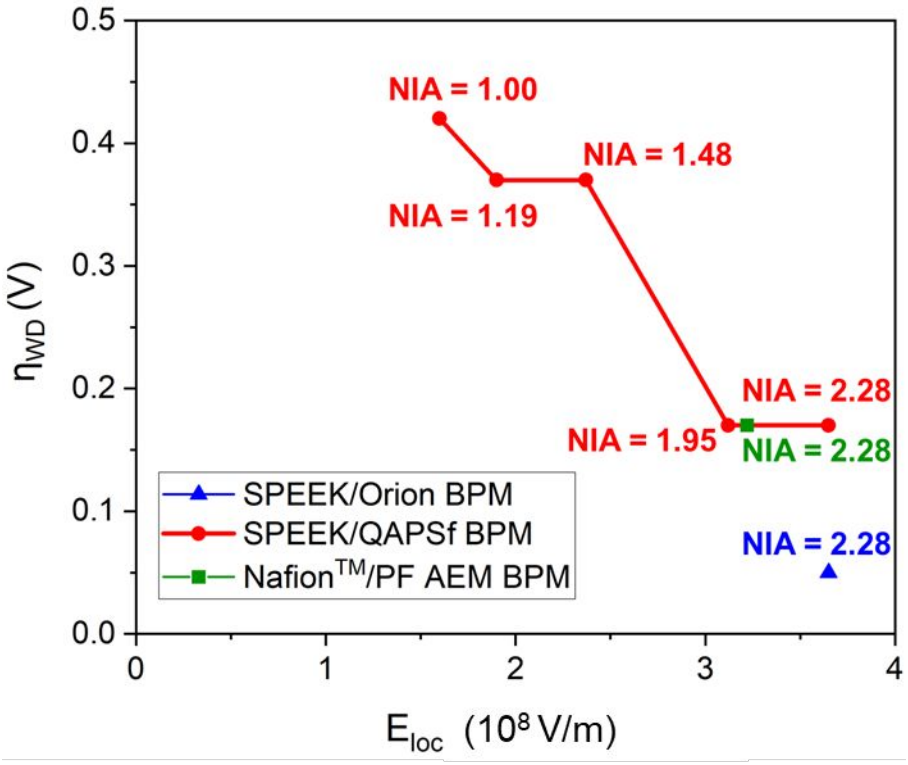

Figure 7. Onset overpotential for water dissociation as a function of local electric field for various BPMs of varying NIA values and IEC values.

Figure 7 plots η_{WD}, determined from **equation 7**, against the E_{loc} value, which was calculated by using the known interfacial area values and constants for t_{dw}, ε and ρ_{BPJ}. The values shown in **Figure 7** are on the same order of magnitude as reported in the literature[7] (i.e., ~ 1x10^8 V m^{-1}) and **equation 7** bares similarity to the equation used by Kohl and co-workers[76] except **equation 7** here captures interfacial area. t_{dw} used in **equation 7** was 20 nm based on literature precedent[17]. ε was based upon available values for Nafion™ [78] and hydrocarbon anion exchange and cation exchange membranes[79]. ε can also be calculated by the weighted average between the polymer materials and water as described in our previous work[80] and others[79]. ρ_{BPJ} was based on the lowest IEC value between the AEM and CEM. The lower IEC value was selected because it dictates the number of oppositely charged pairs that can form in the bipolar junction region. IEC was converted to density by multiplying by the density of the membrane material (1.40 g cm^{-3} for hydrocarbon[81] and 1.58 g cm^{-3} for perfluorinated polymers like Nafion™ [82]). This conversion resulted in an ρ_{IEM} values that ranged from 1.23x10^2 C cm^{-3} to 2.96x10^2 C cm^{-3} depending on the IEC value used (see **equation S1** for an example calculation). **Equation S2** is an example

calculation for E_{loc}. **Figure 7** shows that η_{WD} decreases with increasing the magnitude of E_{loc}. This trend supports that the greater interfacial area increases the strength of E_{loc} that is responsible for the 250 mV drop in onset potential observed in **Figure 4b**.

The limited increase in current density (20 to 50%) with the largest NIA value BPM (NIA = 2.28) was ascribed to mixed kinetics-diffusion control. Using Faraday's Law of Electrolysis (**equation 8**), the change in mass per time can be estimated by the VdC_{H_2O}/dt. Writing the water species conservation of mass equation in the bipolar junction region (**equation 9**) and assuming i.) no convection and Fick's 2nd Law of Diffusion and ii.) a first-order reaction rate law for water splitting (**equation 10**), the current response in Faraday's Law is controlled both by reaction kinetics and diffusion of water to the interface (**equation 11**). Inspection of **equation 11** reveals that the current density response is not explicitly related to interfacial area. The parameter of interfacial area is captured indirectly in k_d^{app} because EIS experiments showed that larger NIA values increased k_d^{app}(**Figure 5c**), but there was some scatter in the upward trend. Hence, improving the current density in the interfacial region of bipolar junctions may require a substantial gain in k_d^{app} (e.g., 2 orders of magnitude) while also curtailing any diffusion limitations. The small to negligible increase in current density for BPMs with smaller NIA values (e.g., 1.19 and 1.48) were attributed to diffusion resistances dominating over kinetics. Once the k_d^{app} value increased by 10-20x, increases in current density occurred.

$$i = -\frac{F}{A_{int}} \cdot \frac{\Delta m_i}{\Delta t} = -\frac{F \cdot V}{A_{int}} \cdot \frac{dC_{H_2O}}{dt} \quad (8)$$

$$\frac{dC_{H_2O}}{dt} = -\nabla \cdot N_{H_2O} + R_{H_2O} \quad (9)$$

$-\nabla \cdot N_{H_2O}$ is simplified to $-D_{H_2O}\frac{d^2C_{H_2O}}{dx^2}$ because convection is negligible and 1-D transport is assumed.

$$H_2O \xrightarrow{BPJ} H^+ + OH^-$$

$$R_{H_2O} = \upsilon_{H_2O} r_{H_2O} = -k_d^{app} C_{H_2O} \quad (10)$$

υ_{H_2O}: stoichiometric coefficient for water is -1.

$$i = F \cdot t_{dw} \cdot \left(D_{H_2O} \frac{d^2 C_{H_2O}}{dx^2} + k_d^{app} C_{H_2O} \right) \quad (11)$$

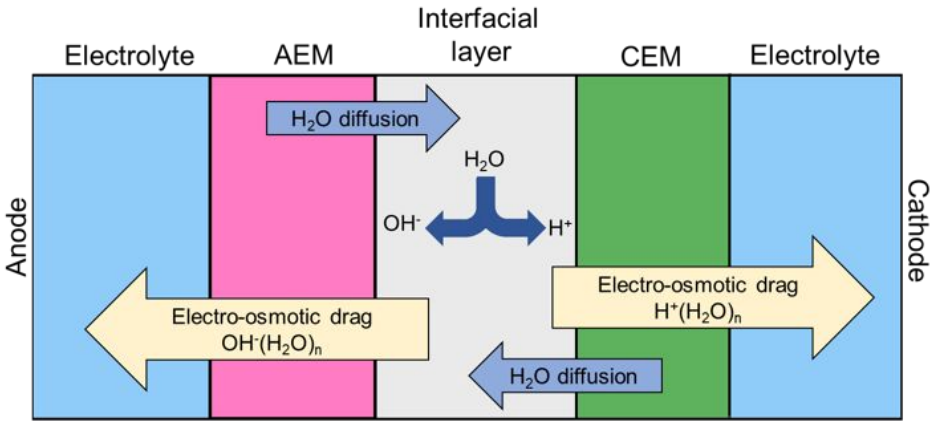

Figure 8. Diffusion of water to the interface and electro-osmotic drag of water away from the interface.

Rapid water delivery to the bipolar junction region in BPMs and avoiding dehydration at the interface[12] is vital for high current density operation in BPMs and long-term stability. Water management in BPMs has not been researched extensively, but most BPMs show relatively low current density values in comparison to their AEM and CEM analogues (i.e., difficulty achieving high current densities > 1.5 A cm^{-2}). It was shown recently by Boettcher and co-workers[12] that BPMs can sustain a high current density with judicious selection of the catalyst at different AEM and CEM layers in BPMs (i.e., using two different catalysts in the interfacial region). However, they also discussed BPM instability due to dehydration. It is important to recognize that every water molecule brought to the bipolar junction interface for splitting in BPMs is accompanied by solvated hydronium and hydroxide ions migrating away from the interface. These solvated ions drag a few water molecules with them. Hence, water diffusion to the interface has to flow against the electro-osmotic drag of ions away from the interface (**Figure 8**). Future work will look to study water management in BPMs and to devise solutions that overcome diffusion limitations that result

in relatively low current density values seen in BPMs when compared to single ion-conducting IEMs used in fuel cells and water electrolyzers. Recently, Boettcher and co-workers demonstrated that a thin CEM appended to an AEM improves water transport to the junction region and enhanced current density[86].

Conclusions

BPMs with systematically controlled interfacial areas were fabricated via soft lithography. This approach for manufacturing BPMs was conducive for a multitude of materials chemistries that are known to have excellent chemical stability at extreme pH values, elevated temperatures (up to 80 °C), and in the presence of oxidizers. By using micropatterned interfaces for SPEEK/QAPSf BPMs, the interfacial area was increased up to 2.28x resulting in a 250 mV reduction in onset potential and 50% improvement in current density at 1.5 V over the non-patterned/flat BPM variant. EIS and simple physics models revealed that the increase in interfacial area amplifies the junction region electric field resulting in lower resistance values for water dissociation (R_w) and a larger apparent water dissociation reaction rate constants (k_d^{app}). The best BPM material was comprised of SPEEK CEM and Orion AEM and this material showed an onset potential at 0.84 V, which was near the thermodynamic minimum, while also displaying significantly lower crossover current when compared against a commercial variant BPM (Fumasep®). Future work will look to fabricate CEM or AEM surfaces with smaller patterned feature sizes in addition to incorporating the respective interfaces with more appropriate metal oxide catalysts[12]. The role of bonding and adhesion in the fabrication of BPMs with high surface area interfaces also requires further investigation – especially in the context of potential mixing and complexation between oppositely charge polymers (e.g., similar to what is observed coacervate materials[83]) and their effect on water splitting in BPMs. These activities may lead to BPMs that facilitate large current density values and thus overcoming barriers that currently stymie BPMs from being deployed in established and emerging electrochemical energy conversion technologies.

Experimental

Materials

The base polymers for making hydrocarbon poly(arylene ether) CEMs and AEMs were poly(ether ether ketone) (PEEK) from Victrex and Udel® poly(arylene ether sulfone) (M_w = 60,000, ACS grade) from Acros Organics. Another type of hydrocarbon AEM, Orion TM1 polymer (medium molecular weight and an all-carbon backbone poly(arylene) chemistry), was sourced as a powder resin from Orion Polymer. The perfluorinated CEM was prepared from Nafion™ dispersion (20 wt% in alcohol-water mixture) sourced from Ion Power. The perfluorinated AEM, Gen 211b, was prepared by the National Renewable Energy Laboratory (NREL)[57]. Commercially available BPM (Fumasep®) was obtained from the Fuel Cell Store.

Materials used for preparing micropatterned PDMS molds were silicon wafer (Purewafer), SU-8 2025 negative photoresist (Microchem), SU-8 developer (Microchem), gamma butyrolactone (GBL) (Sigma-Aldrich) and Sylgard® 184 silicone elastomer base (Dow Corning).

Other chemicals for modifying the base polymers, fabricating membranes, and performing electrochemical experiments and material characterization are: chloroform ($CHCl_3$) (≥ 99.8 %), methanol (MeOH) (≥ 99.8 %), n-methyl-2-pyrrolidone (NMP) (> 99.0 %), 1-methylpyrrolidine (98 %), sulfuric acid (H_2SO_4) (≥ 95 %), chlorotrimethylsilane (≥ 98.0 %), potassium nitrate (KNO_3) (≥ 99.0 %), dimethylsulfoxide (DMSO) (≥ 99.9 %), deuterated dimethylsulfoxide (d6-DMSO) (99.5 %), deuterated chloroform ($CDCl_3$) (99.6 % D), reagent alcohol (90 % ethanol, 5 % methanol, and 5 % 2-propanol), N,N-dimethylformamide (DMF) (≥ 99.8 %), and isopropanol (≥ 99.5 %) obtained from VWR, paraformaldehyde (reagent grade) and stannic chloride ($SnCl_4$) from Sigma-Aldrich, N,N-dimethylacetamide (DMAc) (ACS grade) from Alfa Aesar, and aluminum hydroxide $Al(OH)_3$ Nanopowder (10 nm, 99.9 %) from U.S. Research Nanomaterials, Inc. Deionized (DI) water with 18.2 MΩ resistivity and < 10 ppb TOC (Millipore) was withdrawn within 2 hours of performing an experiment. Ultra-pure nitrogen gas was sourced from Airgas.

Fabrication of micropatterned PDMS molds

A silicon submaster, using the procedure by Arges and co-workers[62, 63], was prepared by a standard photolithography process. In this process, SU-8 2025 resist was diluted with GBL to obtain 55% solid ratio. This solution was spincoated on to a silicon wafer at 2000 rpm for 45 seconds, soft baked at 95 °C for 30 minutes, cooled in a heat insulating cabinet for 30 minutes, and exposed to 225 mJ cm^{-2} UV radiation in presence of a chromium mask that has the desired pattern.

Immediately after exposure, the silicon wafer was baked for 1 minute at 65 °C followed by 1 minute at 95 °C and allowed to cool slowly for 5 minutes. The wafer was developed by immersion in SU-8 developer for 5 minutes with gentle shaking and agitation, quenched in IPA and dried with nitrogen. The resulting wafer was thermally treated at 95 °C for 10 minutes. Finally, PDMS was cured on top of the silicon submaster to obtain the micropatterned PDMS mold by using the following procedure: 10 mL PDMS solution (SYLGARD-184) and 1 mL curing agent were thoroughly mixed and poured onto the silicon submaster kept inside a desiccator. Vacuum was slowly applied to the desiccator and held for 30 mins. It was then heated to 75 °C to cure the PDMS mixture for 40 mins.

Synthesis and chemical characterization of CEMs and AEMs from poly(arylene ethers)

PEEK was converted to SPEEK for preparing CEMs using the procedure by Palakkal *et al* [84]. PSf was processed into AEMs by chloromethylating the PSf via Friedel-Crafts alkylation followed by amination of the chloromethylated PSf (CMPSf) with a tertiary amine[85] to make QAPSf. The scheme for preparing SPEEK and QAPSf is detailed in the SI section. **Figures S9a** and **9b** present the synthesis schemes for SPEEK and QAPSf.

^{1}H NMR spectra of SPEEK, CMPSf, QAPSf are provided under **Figures S10a** to **S10c**. Integration of the NMR spectra allowed for determination of the membranes' ion-exchange capacity. (IEC values; see the SI section for calculations).

Preparation of perfluorinated AEMs and CEMs, and alkaline stable hydrocarbon AEM

Nafion™ dispersion was diluted with reagent alcohol to make a 10 wt% solution. For every 9 mL of 10 wt% Nafion™ dispersion in reagent alcohol, 1 mL of DMF was added. This solution was drop casted on a flat glass plate or patterned PDMS mold and placed in an oven. The oven temperature was maintained at 60 °C overnight (14 hours) followed by a temperature of 120 °C for 2 hours to evaporate the solvents completely. The perfluorinated AEM was used as is.

For the alkaline stable hydrocarbon AEM, Orion resin was dissolved in DMSO to make a 5 wt% solution and drop casted on a flat glass plate in an oven at 60 °C overnight (14 hours)

followed by a temperature of 120 °C for 2 hours to evaporate the solvents completely. After that, the membrane was removed from the plate with the aid of DI water.

Characterization of AEMs and CEMs

The SI details the experimental procedures for measuring ionic conductivity, IEC, transference number, permselectivity, and water uptake. The details for imaging the samples using a scanning electron microscope are also provided in the SI.

Preparation of flat and micropatterned BPMs

For BPMs that contained water dissociation catalysts, a suspension of $Al(OH)_3$ in DI water was spray painted on the CEM and allowed to dry in a fume hood at room temperature (22 to 25 °C). Catalyst loadings were systematically varied from 0.02 mg cm^{-2} to 0.50 mg cm^{-2}. BPMs were fabricated by hot pressing the flat or patterned CEM with an AEM at 5000 lb and 120 °C in a Carver thermal-mechanical press for 30 min. Then, the BPMs were solvent vapor annealed in a custom-built flow chamber[66] at room temperature in a mixture of saturated 2-butanone (or saturated acetone for perfluorinated BPMs) and dry nitrogen. The flow rates were 5 sccm for each stream and the BPMs were annealed for 1 hour. After annealing, the saturated solvent vapor stream was set to 0 sccm and the dry nitrogen stream was increased to 250 sccm for 10 minutes to rapidly remove solvent from the BPM.

Polarization behavior of BPMs

A homemade 4-point cell was prepared to test the polarization behavior of BPMs. **Figure 3b** presents the two-compartment cell for polarization studies of BPMs. Both compartments were filled with 1 M aqueous KNO_3 solution and separated by the BPM. The working and counter electrodes on the potentiostat were attached to platinum wires with Pt-Ir meshes in the 4 point cell (**Figure 3b**). The working electrode from the potentiostat was connected to the Pt-Ir mesh electrode facing the AEM side. The Pt-Ir meshes were immersed in the KNO_3 solution placed in either compartment of the cell. Two Ag/AgCl reference electrodes were placed close to either side

of the BPM using Luggin capillaries. During electrochemical experiments for studying polarization behavior, the working electrode was biased in the positive direction.

A Gamry Reference 3000 Potentiostat/Galvanostat was used for obtaining the polarization curves. Polarization curves were obtained by running chronoamperometry experiments on the BPMs in the voltage range of 0-3 V with a step size of 0.1 V. The voltage was held at a constant value for 15 seconds and the final steady state current at each step was recorded.

Figure S7 shows an example of the method for determining the onset potential for water splitting in BPMs using data analysis and graphing software "Originlab". In this example, the onset potential was 0.92 V and was obtained by the intersection points of the tangents seen on the curve. The application automatically picks a point in the kinetics limited part of the polarization curve with constant slope and another point in the mixed control regime of the curve with a constant slope. It then draws tangents from both points and calculates the intersection of the tangents. This intersection is designated the onset potential.

Acknowledgements

This work was primarily supported by the National Science Foundation (Award # 1703307). Electron microscopy was performed in the LSU Shared Instrumentation Facilities. NMR spectra was collected on NMR spectrometers available in the LSU Department of Chemistry. Silicon submasters were prepared in LSU's Nanofabrication Facility. All the experimental work, minus PF AEM preparation, was performed at LSU. NREL contributed to data analysis, presentation, and writing and supplying PF AEM materials. The NREL contribution was supported by the U.S. Department of Energy under Contract No. DE-AC36-08GO28308 with Alliance for Sustainable Energy, LLC, the Manager and Operator of the National Renewable Energy Laboratory. Funding provided by the U.S. Department of Energy Office of Energy Efficiency and Renewable Energy Fuel Cell Technologies Office. The views and opinions of the authors expressed herein do not necessarily state or reflect those of the United States Government or any agency thereof. Neither the United States Government nor any agency thereof, nor any of their employees, makes any warranty, expressed or implied, or assumes any legal liability or responsibility for the accuracy, completeness, or usefulness of any information, apparatus, product, or process disclosed, or represents that its use would not infringe privately owned rights. The U.S.

Author contributions

S.K. performed all experiments. G.V. synthesized CMPSf. D.B. created Figure 1(a) and assisted with some electron microscopy imaging. L.Z. fabricated the PDMS mold. J.C. assisted with SPEEK synthesis. B.P. supplied PF AEM and reviewed the manuscript. S.K. and C.G.A. designed the experiments, analyzed data, and wrote the manuscript.

List of symbols used

a_{H+}^{PEM} = activity of protons in the PEM

a_{OH-}^{AEM} = activity of hydroxide ions in the AEM

i = current density

k_d^{app} = apparent rate constant for water dissociation

m_i = mass

r_{H_2O} = reaction rate of water

t = time

t_{dw} = depletion region width

x = direction of flow of water and ionic species

A_{int} = interfacial area

C_{H_2O} = concentration of water

D_{H_2O} = diffusion coefficient of water

E_j = junction potential

E_{loc} = local electric field

E_{onset} = onset potential for water dissociation

F = Faraday constant

K_w = water dissociation constant

N_{H_2O} = flux of water molecules

R = universal gas constant

R_{H_2O} = rate of dissociation of water

T = temperature

V = control volume

ε = permittivity of the medium

ε_0 = vacuum permittivity

ε_r = dielectric constant

η_{WD} = water dissociation overpotential

v_{H_2O} = stoichiometric coefficient of water

ρ_{BPJ} = density of fixed charges

ϕ_{BPJ} = local potential

References

1. Strathmann H, Grabowski A, Eigenberger G. Ion-exchange membranes in the chemical process industry. *Industrial & Engineering Chemistry Research* **2013**, 52:10364-10379.
2. Sata T. *Ion Exchange Membranes*; Royal Society of Chemistry, **2004**.
3. Bauer B, Gerner FJ, Strathmann H. Development of bipolar membranes. *Desalination* **1988**, 68:279-292.
4. Strathmann H, Rapp HJ, Bauer B, Bell CM. Theoretical and practical aspects of preparing bipolar membranes. *Desalination* **1993**, 90:303-323.
5. Ramirez P, Rapp HJ, Reichle S, Strathmann H, Mafe S. Current-voltage curves of bipolar membranes. *Journal of Applied Physics* **1992**, 72:259-264.
6. Strathmann H, Krol JJ, Rapp HJ, Eigenberger G. Limiting current density and water dissociation in bipolar membranes. *Journal of Membrane Science* **1997**, 125:123-142.
7. Mafe S, Ramirez P, Alcaraz A. Electric field-assisted proton transfer and water dissociation at the junction of a fixed-charge bipolar membrane. *Chemical Physics Letters* **1998**, 294:406-412.
8. Nikonenko VV, Pismenskaya ND, Belova EI, Sistat P, Huguet P, Pourcelly G, Larchet C. Intensive current transfer in membrane systems: Modelling, mechanisms and application in electrodialysis. *Advances in Colloid and Interface Science* **2010**, 160:101-123.
9. Simons R. Electric field effects on proton transfer between ionizable groups and water in ion-exchange membranes. *Electrochimica Acta* **1984**, 29:151-158.
10. Shen C, Wycisk R, Pintauro PN. High performance electrospun bipolar membrane with a 3D junction. *Energy & Environmental Science* **2017**, 10:1435-1442.
11. Giesbrecht PK, Freund MS. Recent Advances in Bipolar Membrane Design and Applications. *Chemistry of Materials* **2020**, 32:8060-8090.
12. Oener SZ, Foster MJ, Boettcher SW Carbonate dynamics and opportunities with low temperature, anion exchange membrane-based electrochemical carbon dioxide separators. **2020**, 369: 1099-1103.
13. Fu R, Xu T, Wang G, Yang W, Pan Z. PEG–catalytic water splitting in the interface of a bipolar membrane. *Journal of Colloid and Interface Science* **2003**, 263:386-390.
14. Li J, Wang Y, Yang C, Long G, Shen H. Membrane catalytic deprotonation effects. *Journal of Membrane Science* **1998**, 147:247-256.

15. McDonald MB, Freund MS. Graphene Oxide as a Water Dissociation Catalyst in the Bipolar Membrane Interfacial Layer. *ACS Applied Materials & Interfaces* **2014**, 6:13790-13797.
16. McDonald MB, Freund MS, Hammond PT. Catalytic, Conductive Bipolar Membrane Interfaces through Layer-by-Layer Deposition for the Design of Membrane-Integrated Artificial Photosynthesis Systems. *ChemSusChem* **2017**, 10:4599-4609.
17. Yan Z, Zhu L, Li YC, Wycisk RJ, Pintauro PN, Hickner MA, Mallouk TE. The balance of electric field and interfacial catalysis in promoting water dissociation in bipolar membranes. *Energy & Environmental Science* **2018**, 11:2235-2245.
18. Peng F, Peng S, Huang C, Xu T. Modifying bipolar membranes with palygorskite and FeCl3. *Journal of Membrane Science* **2008**, 322:122-127.
19. Fu R-Q, Xue Y-H, Xu T-W, Yang W-H. Fundamental studies on the intermediate layer of a bipolar membrane Part IV. Effect of polyvinyl alcohol (PVA) on water dissociation at the interface of a bipolar membrane. *Journal of Colloid and Interface Science* **2005**, 285:281-287.
20. Xue Y-H, Fu R-Q, Fu Y-x, Xu T-W. Fundamental studies on the intermediate layer of a bipolar membrane V. Effect of silver halide and its dope in gelatin on water dissociation at the interface of a bipolar membrane. *Journal of Colloid and Interface Science* **2006**, 298:313-320.
21. Rajesh AM, Chakrabarty T, Prakash S, Shahi VK. Effects of metal alkoxides on electro-assisted water dissociation across bipolar membranes. *Electrochimica Acta* **2012**, 66:325-331.
22. Nagasubramanian K, Chlanda FP, Liu K-J. Use of bipolar membranes for generation of acid and base - an engineering and economic analysis. *Journal of Membrane Science* **1977**, 2:109-124.
23. Mani KN. Electrodialysis water splitting technology. *Journal of Membrane Science* **1991**, 58:117-138.
24. Lu H, Wang L, Wycisk R, Pintauro PN, Lin S. Quantifying the kinetics-energetics performance tradeoff in bipolar membrane electrodialysis. *Journal of Membrane Science* **2020**:118279.
25. Chen B, Jiang C, Wang Y, Fu R, Liu Z, Xu T. Selectrodialysis with bipolar membrane for the reclamation of concentrated brine from RO plant. *Desalination* **2018**, 442:8-15.
26. Strathmann H. *Ion-Exchange Membrane Separation Processes, Volume 9*. Vol. 9. Amsterdam, The Netherlands: Elsevier Science; **2004**.
27. Bazinet L, Lamarche F, Ippersiel D. Bipolar-membrane electrodialysis: applications of electrodialysis in the food industry. *Trends in Food Science & Technology* **1998**, 9:107-113.
28. Quoc AL, Lamarche F, Makhlouf J. Acceleration of pH Variation in Cloudy Apple Juice Using Electrodialysis with Bipolar Membranes. *Journal of Agricultural and Food Chemistry* **2000**, 48:2160-2166.
29. Vera E, Sandeaux J, Persin F, Pourcelly G, Dornier M, Ruales J. Deacidification of passion fruit juice by electrodialysis with bipolar membrane after different pretreatments. *Journal of Food Engineering* **2008**, 90:67-73.
30. Papageorgopoulos D. Fuel Cell R&D Overview. **2019**. Available at: https://www.hydrogen.energy.gov/pdfs/review19/plenary_fuel_cell_papageorgopoulos_2019.pdf.

31. Seeberger D, McLaughlin D, Hauenstein P, Thiele S. Bipolar-interface fuel cells – an underestimated membrane electrode assembly concept for PGM-free ORR catalysts. *Sustainable Energy & Fuels* **2020**, 4:2508-2518.
32. Xu X, Peng S, Lu S, Gong J, Zhang J, Huang W, Xiang Y. Modulation of the microstructure of the Ag/C-based alkaline cathode via the ionomer content for a bipolar membrane fuel cell. *Journal of Power Sources* **2017**, 354:92-99.
33. Arges CG, Prabhakaran V, Wang L, Ramani V. Bipolar polymer electrolyte interfaces for hydrogen-oxygen and direct borohydride fuel cells. *International Journal of Hydrogen Energy* **2014**, 39:14312-14321.
34. Sheng W, Gasteiger HA, Shao-Horn Y. Hydrogen oxidation and evolution reaction kinetics on platinum: Acid vs alkaline electrolytes. *Journal of the Electrochemical Society* **2010**, 157:B1529-B1536.
35. Mustain WE, Kepler K, Prakash J. CoPdx oxygen reduction electrocatalysts for polymer electrolyte membrane and direct methanol fuel cells. *Electrochimica Acta* **2007**, 52:2102-2108.
36. Mustain WE, Prakash J. Kinetics and mechanism for the oxygen reduction reaction on polycrystalline cobalt–palladium electrocatalysts in acid media. *Journal of Power Sources* **2007**, 170:28-37.
37. Li R, Wei Z, Gou X. Nitrogen and Phosphorus Dual-Doped Graphene/Carbon Nanosheets as Bifunctional Electrocatalysts for Oxygen Reduction and Evolution. *ACS Catalysis* **2015**, 5:4133-4142.
38. Arges CG, Prabhakaran V, Wang L, Ramani V. Bipolar polymer electrolyte interfaces for hydrogen–oxygen and direct borohydride fuel cells. *International Journal of Hydrogen Energy* **2014**, 39:14312-14321.
39. Wang Z, Parrondo J, He C, Sankarasubramanian S, Ramani V. Efficient pH-gradient-enabled microscale bipolar interfaces in direct borohydride fuel cells. *Nature Energy* **2019**, 4:281-289.
40. Braesch G, Wang Z, Sankarasubramanian S, Oshchepkov AG, Bonnefont A, Savinova ER, Ramani V, Chatenet M. A high performance direct borohydride fuel cell using bipolar interfaces and noble metal-free Ni-based anodes. *Journal of Materials Chemistry A* **2020**.
41. Wang Z, Mandal M, Sankarasubramanian S, Huang G, Kohl PA, Ramani VK. Influence of Water Transport Across Microscale Bipolar Interfaces on the Performance of Direct Borohydride Fuel Cells. *ACS Applied Energy Materials* **2020**, 3:4449-4456.
42. Salvatore DA, Weekes DM, He J, Dettelbach KE, Li YC, Mallouk TE, Berlinguette CP. Electrolysis of Gaseous CO2 to CO in a Flow Cell with a Bipolar Membrane. *ACS Energy Letters* **2018**, 3:149-154.
43. Li YC, Yan Z, Hitt J, Wycisk R, Pintauro PN, Mallouk TE. Bipolar Membranes Inhibit Product Crossover in CO_2 Electrolysis Cells. *Advanced Sustainable Systems* **2018**, 2:n/a.
44. Chen Y, Vise A, Klein WE, Cetinbas FC, Myers DJ, Smith WA, Deutsch TG, Neyerlin KC. A Robust, Scalable Platform for the Electrochemical Conversion of CO2 to Formate: Identifying Pathways to Higher Energy Efficiencies. *ACS Energy Letters* **2020**, 5:1825-1833.
45. Patru, A, Binninger, T, Pribyl, B, Schmidt, T.J. Design Principles of Bipolar Electrochemical Co-Electrolysis Cells for Efficient Reduction of Carbon Dioxide from Gas Phase at Low Temperature. *Journal of the Electrochemical Society*. **2019**, 166: F34-F43

46. Rigdon WA, Omasta TJ, Lewis C, Hickner MA, Varcoe JR, Renner JN, Ayers KE, Mustain WE. Carbonate dynamics and opportunities with low temperature, anion exchange membrane-based electrochemical carbon dioxide separators. *Journal of Electrochemical Energy Conversion and Storage* **2017**, 14:020701/020701-020701/020708.
47. Simons R. A novel method for preparing bipolar membranes. *Electrochimica Acta* **1986**, 31:1175-1176.
48. Simons R. Preparation of a high-performance bipolar membrane. *Journal of Membrane Science* **1993**, 78:13-23.
49. Unlu M, Zhou J, Anestis-Richard I, Kohl PA. Characterization of anion exchange ionomers in hybrid polymer electrolyte fuel cells. *ChemSusChem* **2010**, 3:1398-1402.
50. Chen Y, Wrubel JA, Klein WE, Kabir S, Smith WA, Neyerlin KC, Deutsch TG. High-Performance Bipolar Membrane Development for Improved Water Dissociation. *ACS Applied Polymer Materials* **2020**.
51. Jeon Y, Kim DJ, Koh JK, Ji Y, Kim JH, Shul Y-G. Interface-designed Membranes with Shape-controlled Patterns for High-performance Polymer Electrolyte Membrane Fuel Cells. *Scientific Reports* **2015**, 5:16394.
52. Bae JW, Cho Y-H, Sung Y-E, Shin K, Jho JY. Performance enhancement of polymer electrolyte membrane fuel cell by employing line-patterned Nafion membrane. *Journal of Industrial and Engineering Chemistry* **2012**, 18:876-879.
53. Zhou Z, Dominey RN, Rolland JP, Maynor BW, Pandya AA, DeSimone JM. Molded, High Surface Area Polymer Electrolyte Membranes from Cured Liquid Precursors. *Journal of the American Chemical Society* **2006**, 128:12963-12972.
54. Jang S, Her M, Kim S, Jang J-H, Chae JE, Choi J, Choi M, Kim SM, Kim H-J, Cho Y-H, et al. Membrane/Electrode Interface Design for Effective Water Management in Alkaline Membrane Fuel Cells. *ACS Applied Materials & Interfaces* **2019**, 11:34805-34811.
55. Arges CG, Kambe Y, Dolejsi M, Wu G-P, Segal-Pertz T, Ren J, Cao C, Craig GSW, Nealey PF. Interconnected ionic domains enhance conductivity in microphase separated block copolymer electrolytes. *Journal of Materials Chemistry A* **2017**, 5:5619-5629.
56. Gotrik KW, Hannon AF, Son JG, Keller B, Alexander-Katz A, Ross CA. Morphology Control in Block Copolymer Films Using Mixed Solvent Vapors. *ACS Nano* **2012**, 6:8052-8059.
57. Park AM, Owczarczyk ZR, Garner LE, Yang-Neyerlin AC, Long H, Antunes CM, Sturgeon MR, Lindell MJ, Hamrock SJ, Yandrasits MA, et al. Synthesis and characterization of perfluorinated anion exchange membranes. *ECS Transactions* **2017**, 80:957-966.
58. Kusoglu A, Weber AZ. New Insights into Perfluorinated Sulfonic-Acid Ionomers. *Chemical Reviews* **2017**, 117:987-1104.
59. Lee W-H, Kim YS, Bae C. Robust Hydroxide Ion Conducting Poly(biphenyl alkylene)s for Alkaline Fuel Cell Membranes. *ACS Macro Letters* **2015**, 4:814-818.
60. Lee W-H, Mohanty AD, Bae C. Fluorene-Based Hydroxide Ion Conducting Polymers for Chemically Stable Anion Exchange Membrane Fuel Cells. *ACS Macro Letters* **2015**, 4:453-457.
61. Arges C, Wang L, Parrondo J, Ramani V. Best Practices for Investigating Anion Exchange Membrane Suitability for Alkaline Electrochemical Devices: Case Study Using Quaternary Ammonium Poly(2,6-dimethyl 1,4-phenylene)oxide Anion Exchange Membranes. *Journal of the Electrochemical Society* **2013**, 160:F1258-F1274.

62. Moruno FL, Rubio JE, Atanassov P, Cerrato JM, Arges CG, Santoro C. Microbial desalination cell with sulfonated sodium (poly(ether ether ketone) as cation exchange membranes for enhancing power generation and salt reduction. *Bioelectrochemistry* **2018**, 121:176-184.
63. Moruno FL, Rubio JE, Santoro C, Atanassov P, Cerrato JM, Arges CG. Investigation of patterned and non-patterned poly(2,6-dimethyl 1,4-phenylene) oxide based anion exchange membranes for enhanced desalination and power generation in a microbial desalination cell. *Solid State Ionics* **2018**, 314:141-148.
64. Zhang L, Porter T, Guillory S, Cao C, Arges CG. Patterning polymer electrolyte membranes for fuel cell and electrolysis applications. *ECS Transactions* **2017**, 77:1325-1335.
65. Wilhelm FG, Pünt I, van der Vegt NFA, Strathmann H, Wessling M. Asymmetric Bipolar Membranes in Acid−Base Electrodialysis. *Industrial & Engineering Chemistry Research* **2002**, 41:579-586.
66. Arges CG, Kambe Y, Suh HS, Ocola LE, Nealey PF. Perpendicularly Aligned, Anion Conducting Nanochannels in Block Copolymer Electrolyte Films. *Chemistry of Materials* **2016**, 28:1377-1389.
67. Manohar M, Das AK, Shahi VK. Efficient Bipolar Membrane with Functionalized Graphene Oxide Interfacial Layer for Water Splitting and Converting Salt into Acid/Base by Electrodialysis. *Industrial & Engineering Chemistry Research* **2018**, 57:1129-1136.
68. Manohar M, Shukla G, Pandey RP, Shahi VK. Efficient bipolar membrane with protein interfacial layer for optimal water splitting. *Journal of Industrial and Engineering Chemistry* **2017**, 47:141-149.
69. Arges CG, Zhang L. Anion Exchange Membranes' Evolution toward High Hydroxide Ion Conductivity and Alkaline Resiliency. *ACS Applied Energy Materials* **2018**, 1:2991-3012.
70. Arges CG, Ramani V. Two-dimensional NMR spectroscopy reveals cation-triggered backbone degradation in polysulfone-based anion exchange membranes. *Proceedings of the National Academy of Sciences* **2013**, 110:2490-2495.
71. Arges CG, Ramani V. Investigation of cation degradation in anion exchange membranes using multi-dimensional NMR spectroscopy. *Journal of the Electrochemical Society* **2013**, 160:F1006-F1021.
72. Bauer B, Strathmann H, Effenberger F. Anion-exchange membranes with improved alkaline stability. *Desalination* **1990**, 79:125-144.
73. Arges CG, Wang L, Jung M-s, Ramani V. Mechanically Stable Poly(arylene ether) Anion Exchange Membranes Prepared from Commercially Available Polymers for Alkaline Electrochemical Devices. *Journal of the Electrochemical Society* **2015**, 162:F686-F693.
74. Kang M-S, Choi Y-J, Kim S-H, Moon S-H. Enhancement of water splitting in bipolar membranes by optimized composite anion-exchange layer and alkali-treated polyacrylonitrile catalytic junction. *Journal of Membrane Science* **2004**, 229:137-146.
75. Park HB, Freeman BD, Zhang Z-B, Sankir M, McGrath JE. Highly Chlorine-Tolerant Polymers for Desalination. *Angewandte Chemie International Edition* **2008**, 47:6019-6024.
76. Ünlü M, Zhou J, Kohl PA. Hybrid Anion and Proton Exchange Membrane Fuel Cells. *The Journal of Physical Chemistry C* **2009**, 113:11416-11423.
77. Newman J, Thomas-Alyea KE. *Electrochemical Systems*. 3rd Edition ed: Wiley; **2004**.

78. Chang K, Luo H, Geise GM. Water content, relative permittivity, and ion sorption properties of polymers for membrane desalination. *Journal of Membrane Science* **2019**, 574:24-32.
79. Kamcev J, Paul DR, Freeman BD. Effect of fixed charge group concentration on equilibrium ion sorption in ion exchange membranes. *Journal of Materials Chemistry A* **2017**, 5:4638-4650.
80. Lei Q, Li K, Bhattacharya D, Xiao J, Kole S, Zhang Q, Strzalka J, Lawrence J, Kumar R, Arges C. Counterion condensation or lack of solvation? Understanding the activity of ions in thin film block copolymer electrolytes. *Journal of Materials Chemistry A* **2020**, 8: 15962-15975
81. Mendil-Jakani H, Lopez IZ, Legrand P, Mareau V, Gonon L. A new interpretation of SAXS peaks in sulfonated poly (ether ether ketone)(sPEEK) membranes for fuel cells. *Physical Chemistry Chemical Physics* **2014**, 16:11243-11250.
82. Zook LA, Leddy J. Density and Solubility of Nafion: Recast, Annealed, and Commercial Films. *Analytical Chemistry* **1996**, 68:3793-3796.
83. Priftis D, Farina R, Tirrell M. Interfacial Energy of Polypeptide Complex Coacervates Measured via Capillary Adhesion. *Langmuir* **2012**, 28:8721-8729.
84. Palakkal VM, Rubio JE, Lin YJ, Arges CG. Low-resistant ion-exchange membranes for energy efficient membrane capacitive deionization. *ACS Sustainable Chemistry & Engineering* **2018**, 6:13778-13786.
85. Palakkal VM, Valentino L, Lei Q, Kole S, Lin YJ, Arges CG. Advancing electrodeionization with conductive ionomer binders that immobilize ion-exchange resin particles into porous wafer substrates. *npj Clean Water* **2020**, 3:5.
86. Oener SZ, Twight LP, Lindquist GA, & Boettcher SW. Thin Cation-Exchange Layers Enable High-Current-Density Bipolar Membrane Electrolyzers via Improved Water Transport. *ACS Energy Letters* **2020**, 6, 1-8.